Intracranial aneurismal pulsatility as a new individual criterion for rupture risk evaluation: Biomechanical and numerical approach (IRRAs project).

Mathieu Sanchez, Omer Ecker, Dominique Ambard, Franck Jourdan, Franck Nicoud, Simon Mendez, J. Lejeune, L. Thines, H. Dufour, H. Brunel, et al.

Intracranial aneurismal pulsatility as a new individual criterion for rupture risk evaluation: Biomechanical and numerical approach (IRRAs project).

M. Sanchez[1, 3] PhD, O. Ecker[2] MD, D. Ambard[3] PhD, F. Jourdan[3] PhD,
F. Nicoud[4] PhD, S. Mendez[4] PhD, J. Lejeune[5] MD, PhD, L. Thines[5] MD, PhD, H. Dufour[6] MD, PhD, H. Brunel[7] MD, P. Machi[2] MD, K. Lobotesis[8] MBBS
A. Bonafe[2] MD, PhD, V. Costalat[2] MD, PhD

[1]Philips Healthcare, France
[2]CHU Montpellier Neuroradiology, France
[3] CNRS-LMGC Montpellier, France
[4] CNRS-I3M Montpellier, France
[5] CHU Lille Neurosurgery, France
[6] CHU Marseille Neurosurgery, France
[7] CHU Marseille Neuroradiology, France
[8] Imperial College Healthcare NHS Trust

Keywords: FSI, cerebral aneurysm, rupture risk, pulsatility

Word count: Main text = 3305 (Abstract = 198)

Contact information:

Mathieu SANCHEZ, PhD (mathieu.sanchez@univ-montp.fr)

LMGC – UMR5508 – Université Montpellier 2 CC048 Place Eugène Bataillon 34095 Montpellier cedex 5 France

All authors have made substantial contributions to all of the following:

(1) the conception and design of the study ; MS, VC, DA, FJ, FN, SM.

(2) acquisition of data ;MS, OE, JL, LT, HD, HB, PM, AB.

(3) analysis and interpretation of data; MS,OE, VC, AB

(4) drafting the article or revising it critically for important intellectual content ; MS, OE, VC, DA, FJ, FN, SM, KL

Itemized list of Tables and Figures

We certify that this manuscript has not been previously published, nor is being considered in whole or in part in any other primary scientific journal. All the authors are aware of and agree to the content of the manuscript. None of the authors have any conflict of interest to declare.

Abstract

Objective: This study was designed to highlight by means of numerical simulations, the correlation between aneurism sac pulsatility and the risk of rupture through the mechanical properties of the wall.

Methods: In accordance to previous work suggesting a correlation between the risk of rupture and the material properties of cerebral aneurysms, twelve fluid-structure interaction (FSI) computations were performed on 12 ”patient-specific” cases, corresponding to typical shapes and locations of cerebral aneurysms.

The variations of the aneurismal volume during the cardiac cycle (ΔV) are compared using wall material characteristics of either degraded and non-degraded tissues.

Results: Aneurysms were located on 7 different arteries: Middle Cerebral Artery (4), Anterior Cerebral Artery (3), Internal Carotid Artery (1), Vertebral Artery (1), Ophthalmic Artery (1) and Basilar Artery (1). Aneurysms presented different shapes (uniform or multi-lobulated) and diastolic volumes (from 18 to 392 mm^3). The pulsatility ($\Delta V/V$) was significantly larger for a soft aneurismal material (average of 26 %) than for a stiff material (average of 4 %). The difference between ΔV, for each condition, was statistically significant: $p = 0.005$.

Conclusion: The difference in aneurismal pulsatility as highlighted in this work might be a relevant patient-specific predictor of aneurysm risk of rupture.

1 Introduction

Intracranial Aneurysm kills about 15 000 people in Europe each year. Most of these people are young, between 40 and 60 years old. New medical imaging techniques are now able to clearly depict intracranial aneurysm, but no systematic screening of this disease exists at the moment. The main reason is that 2 to 6% of the general population lives with an aneurysm (Wardlaw *et al.* [1]), but only 0.5% of them will rupture. Screening of intracranial aneurysm is not justified unless being able to detect the vulnerable aneurysms. Subarachnoid hemorrhage is the consequence of aneurysm rupture and approximately 12% of patients die before receiving medical attention, 40% of the patient will die within the first month and 30% will present a severe permanent disability. Nevertheless, with brain imaging being more frequently and widely used, a growing number of intracranial aneurysms are being diagnosed, raising the problem of which aneurysms harbour a sufficiently high risk of rupture to merit a prophylactic repair. This question is still unsolved at the moment and therapeutic decision for unruptured aneurysm still a challenging point discussed by the neurosurgeon/neuro-interventionist based on sparse epidemiological clinical data that cannot represent the specific individual risk of the patient.

Recent publications have addressed this issue and have demonstrated that, among other variables affecting the natural history of aneurysms, size and location represent independent predictors of both risk of rupture and surgical/endovascular repair outcomes[2, 3]. Other parameters, such as irregular aneurysm shape and the presence of blebs are recognized as markers of weak wall structure and high risk of rupture. Rapid aneurysm growth is also likely a risk factor for rupture[4].

From a mechanical point of view, the rupture of an aneurysm occurs when wall tension exceeds the strength of the wall tissue. Since these quantities cannot be assessed via conventional medical imaging, a natural approach is to compute the wall tension and set a rupture threshold.

Few studies consider the coupled fluid - structure interaction problem (FSI), where the flow equations for blood are solved together with the structural equations for the tissue[5]. The problem is the lack of data on

mechanical properties of cerebral arteries and aneurysms, most of the studies based on a FSI[6-10] framework do not use experimental mechanical behavior of the aneurysm wall as input. A few exceptions exist for the case of the abdominal aorta aneurysms [11, 12] but not for intracranial aneurysms, until recently where in a study by Costalat et al [13], the aneurysm wall properties were characterized and a classification of aneurysm wall behavior was carried out. One of the main conclusions of this work was that the clinical status of the aneurysm (unruptured, pre-ruptured and ruptured) was strongly correlated with the mechanical behavior of the aneurysm wall and hence a classification was proposed, (stiff, intermediate and soft).

This was followed with FSI computations by Sanchez et al. [14], who demonstrated for one specific aneurysm that the different mechanical properties of the aneurysm wall (stiff or soft) are responsible for significantly different variations in aneurism volume over the cardiac cycle (pulsatility). A parametric study was also achieved in this work, and demonstrated that uncertainties did not change the main conclusion.

The further application of these results to the in-vivo setting and in particular to cerebral aneurysms arising from the circle of Willis circle is an additional important step.

The aim of this work was to investigate and verify the correlation between wall biomechanical properties (stiff and soft) and aneurismal volume variation during the cardiac cycle for a variety of aneurysms which differ in shape and location in the circle of Willis.

This study was conceived and carried out as part of the IRRAs consortium which is a research project dedicated to the evaluation of patient-specific risk of rupture of cerebral aneurysms. The consortium brings together neurosurgeons, neuroradiologists and researchers in biomechanical engineering in a common translational research project.

2 Materials and Methods

2.1 Identification of mechanical behavior of aneurysm wall

The details of the study establishing the correlation between the aneurysm status and tissue mechanical properties are given in the work of Costalat et al. [13]. The methodology and main results are briefly given in the following for the sake of completeness. A similar study has been done by Duprey and al. [15] for the thoracic aortic aneurysms.

Each sample was then studied as appropriate for biomaterials[16-19] . Only the meridional axis of the aneurysm was chosen in order to preserve maximum length of the aneurismal tissue in the sample, given the very small size of each specimen and the fragility of the tissue. Using theses measurement series, a model of the tissue behavior was proposed for large displacements in order to represent the evolution of the stress in the materials [20]. For this purpose the assumption that the material is isotropic and non-compressible was made and the hyperelastic model of Mooney-Rivlin with 3 parameters was selected (1). It reads:

$$W = C_{10}(I_1 - 3) + C_{01}(I_2 - 3) + C_{11}(I_1 - 3)(I_2 - 3), \qquad (1)$$

where W is the strain energy potential, $I_1 = tr(\boldsymbol{C})$ and $I_2 = 1/2\,(tr^2(\boldsymbol{C}) - tr(\boldsymbol{C}^2))$ are the first and second strain invariants of the right Cauchy-Green deformation tensor $\boldsymbol{C}$ and C_{10}, C_{01}, C_{11} are the material coefficients.

All unruptured aneurysms presented as stiffer tissue than the ruptured aneurysms.

Their mechanical behavior was either stiff or intermediate. Conversely, all ruptured aneurysms correspond to a soft tissue. The corresponding parameters are given in Table 1 while the strain/stress curves are displayed in Fig. 1.

2.2 Numerical Method

2.2.1 Aneurismal geometry

Aneurysm geometry was obtained from 3D rotational angiography. Using dedicated software ScanIP (Simpleware), the aneurismal geometries were clean up by keeping only the aneurysms and the parent vessels in order to reduce the region of interest. A low-pass filter was applied on the geometries to reduce noise-to-signal ratio. The results were exported as STL files in order to proceed to numerical analysis.

2.2.2 Simulation parameters

The flow boundary conditions imposed were obtained from specific patient examinations by using phase contrast MRI for each aneurysm location (SIEMENS 3T, Skyra, Hessen, Germany). The velocity profiles were considered as uniform. Outlet pressure was computed by computational fluid dynamic (CFD) and used as boundary conditions at the outlet of the computational domain. It had been obtained by resolving the 1D equations in the arterial network with boundary flow conditions from imaging measurement[21].

An intracranial pressure of 20 *mmHg*[22] was applied on the external surface of the geometries to recreate the *in vivo* conditions.

2.2.3 Physical modeling

The blood flow within the computational domain is described by the incompressible Navier-Stokes equations (2), (3).

$$\rho_f \frac{dvf}{dt} = \boldsymbol{div}\,\sigma^f, \qquad (2)$$

$$div\,(\boldsymbol{v_f}) = 0\,, \qquad (3)$$

where $\boldsymbol{v_f}$ is the time dependent flow velocity vector, ρ_f is the density of blood and σ^f is the stress tensor for the fluid part. The flow is assumed to be laminar, a reasonable assumption given the moderate value of the Reynolds number ($Re \approx 300$). Blood is modeled as a Newtonian fluid (4), of density of $\rho_f = 1050$ kg/m^3 and dynamic viscosity of $\mu = 0.004$ Pa.s [9, 23-25].

$$\sigma^f = -p\mathbf{I} + 2\mu\mathbf{D}, \qquad (4)$$

where p is the pressure, **I** is the identity tensor and **D** is the rate of deformation tensor.

For the parent artery, a linear elastic model was selected in order to focus the attention on the aneurismal sac and to reduce the computational time. The structural equation solved for both the artery and aneurismal sac reads (5):

$$\rho_s \frac{\partial \boldsymbol{vs}}{\partial t} = \boldsymbol{div}\ \sigma^s \qquad (5)$$

where σ^s is the Cauchy strain for the structural part and $\boldsymbol{v_s}$ stands for the structural velocity vector.

The aneurysm wall is modeled as an isotropic incompressible hyperelastic material (6):

$$\sigma^s = \rho_s \boldsymbol{F} \frac{\partial W}{\partial \boldsymbol{E}} \boldsymbol{F}^t - p\boldsymbol{I}\,, \qquad (6)$$

where **F** is the transformation gradiant tensor, **E** is the Green Lagrangian strain tensor and W is the strain energy potential defined in Eq.(1) .

The material used for the parent artery has the following properties: Young modulus E = 3 MPa, Poisson ratio v = 0.49, specific mass ρ_s = 2300 kg/m3 and thickness e_{pa} = 0.6 mm [24, 26] .The thickness of the aneurism

wall is e = 0.38 mm. A linear model was used for the arterial wall because the deformations are small enough in all cases (< 5%) to stay in the small deformation theory.

Furthermore, the edge nodes of the arterial extremities are taken away of the displacement in the longitudinal direction

2.2.4 FSI computations

Computations were performed using the software Ansys V.13. The fluid motion equations were solved with the software CFX, which uses the finite volume approach and the Newton-Raphson method for solving the subsequent non-linear system. For the structural part, Ansys employed the finite-element method and the Newton-Raphson algorithm. The wall pressure resulting from the fluid was imported as boundary conditions in the structural analysis while wall displacement calculated by the structure solver was imported as a boundary condition for the fluid solver; this procedure was carried out in an iterative manner within each time step. It was an iterative implicit coupling. At the interface of the two physical domains, the element type differs and the nodes of the two meshes did not coincide, so surface interpolation was carried out[27]. For each FSI computation, a time step of 0.004 s was used. The structural meshes were composed by 2500 to 5000 shell elements and the fluid meshes by 100 000 to 300 000 tetrahedral elements. These meshes were fine enough to ensure the convergence of the computations. The two FSI computations of the reference case from Sanchez et al [14] were performed for mesh refinements multiplied by 10 (about 30 000 elements for structural mesh and 1 000 000 elements for fluid mesh). Despite a significant increase of the computation time, the results were similar. For example, in the soft case, the maximal mesh displacement was 0.78 instead of 0.77 mm (variation of 1.3%) and the volume variation was 44.3 mm^3 instead of 44 mm^3 (variation of 0.7%).

A structural computation was performed before the FSI computation to determine the stress state of the acquired geometry. All the details about the initial stress of the aneurysm geometry are given in Sanchez et al [14].

2.2.5 Wall motion analysis

For each aneurismal geometry, two FSI computations were performed using the two different biomechanical properties (stiff and soft) defined in section 2.1. Volume variations and wall motions were calculated for each aneurysm. For each case, the systolo-diastolic variation of the volume of the aneurysm (ΔV) was computed from the results. The maximal mesh displacement on the aneurysm sac D_{max} was also calculated. ΔV is a global information about the aneurismal sac behaviour, whereas D_{max} provides a local information (maximal displacement of a point of the aneurysm boundary).

In order to compare ΔV and D_{max} between soft and stiff material for different aneurysms, we defined the following ratio:

$$R_v = \Delta V^{soft} / \Delta V^{stiff}$$

$$R_d = D_{max}{}^{soft} / D_{max}{}^{stiff}$$

A pulsatility index was also defined as: $Pulsatility = \Delta V/V$, where V is the diastolic volume of the aneurismal sac.

2.3 Statistical analysis

A statistical analysis was performed to evaluate the influence of ΔV and D_{max} in soft and stiff cases. The comparison was made by using non-parametric Wilcoxon rank test for continuous variables and Fisher exact test for categorical ones. Statistical significance threshold was set at 5%. Statistical analyses were performed using SAS version 9.1 (SAS Institute, Cary, North Carolina).

3 Results

3.1 Aneurysm population

Twelve aneurysms from twelve different patients were computed with the stiff and the soft materials. These aneurysms were located on 7 different arteries: Middle Cerebral Artery right and left (MCA R and L) [4 cases], Anterior Cerebral Artery (ACA) [3 cases], Internal Carotid Artery (ICA) [1 case], Vertebral Artery (VA) [1 case], Ophthalmic Artery (OA) [1 case] and Basilar Artery (BA) [2 cases]. These had a variety of shapes: simple (uniform) or complex (multi-lobulated). The volume varied from 18 mm^3 to 392 mm^3. Geometric information is displayed in Table 2.

3.2 Wall motion results

Fig.2 gives an example of the FSI results for 3 different cases, by displaying maximum displacement for the simulations with soft or stiff materials. All results of the patient-specific FSI computations are displayed in Table 3 and Table 4. Two aneurysms (5 and 6) show unusual results. For aneurysm 5, the volume variation is 149 mm^3. The important initial volume of the aneurysm sac, almost 400 mm3, can explain this important variation. This aneurysm could be considered as a giant aneurysm. Nevertheless, the pulsatility ratio is still in the range of 30% in comparison to an overall mean of 25% for the cases. For aneurysm 6, the pulsatility is much more important than in the other cases. That is the result of a volumetric flow rate more important in this location (vertebral artery) for this specific patient compare to the others (table 4). This due to the particularity of his cerebral arterial network.

A significant difference was observable between ΔV for a stiff material and for a soft material ($p = 0.005$). Consequently, the pulsatility index ($\Delta V / V$) was obviously more important for a soft aneurismal sac (average

of 26 %) than for a stiff aneurismal sac (average of 4 %), in spite of the relatively small number of aneurysms considered.

Naturally, we found the same difference for the ratio R_v: R_v varies from 4 (aneurysm 7 and 10) to 16 (aneurysm 2) for an average of 7. R_d also showed differences between stiff and soft materials but to a lesser extent: the minimum is 1.5 (aneurysm 6) and the maximum is 5 (aneurysm 4) and the average was 3 (Table 5). The difference between ΔV and D_{max} for each condition was statistically significant: $p = 0.005$ for ΔV and $p = 0.02$ for D_{max}.

4 Discussion

Our results clearly suggest that the wall displacement provides information about the level of degradation of the aneurysm wall and, thanks to the findings of Costalat et al [13], about the rupture risk of the aneurysm sac. Our study shows that whatever the location of the aneurysm on the Willis circle, the aneurismal pulsatility was about 7 times higher for soft/ruptured aneurysms in comparison with stiff/unruptured aneurysms (26 % versus 4 %). That is the result of a volumetric flow rate more important in this location (vertebral artery) compare to the others (table 4). These observations are consistent with our previous work: the study from Sanchez et al[14], using FSI computations, where a significant difference between the displacements and volume variations corresponding to the soft (close to the rupture) and stiff (undegraded) tissues was observed in a particular case. This result is generalized to the entirety of the circle of Willis in this paper.

Interestingly, Hayakawa et al [28] highlighted in an observational study on 51 patients using 4D computed tomography angiography (CTA)[28] that the pulsation of the aneurysm sac (or volume variation) between ruptured aneurysms and unruptured aneurysms was significantly different. In their study, 12/51 cerebral aneurysms were ruptured (RCA). Among these 12 RCA, a pulsation was observed in nine cases (75%). Thirty nine cerebral aneurysms were unruptured (URCA); among these 39 URCA, a pulsation was observed in 12 cases (30%). Two of these 12 pulsating URCA were treated by surgery because of the clinical background of the patients. They came to the conclusion that the detection of pulsation in an unruptured aneurysm could be therefore a clue of an important risk factor. Our results confirm this point of view.

Furthermore, the precision needed to identify the aneurismal wall motion variation between unruptured/ruptured aneurysm would be about 0.1 *mm* (D_{max}) or 0.5 mm^3 (ΔV) according to our study. New imaging techniques may approach this high resolution level in recent literature (for example Ishida et al [29] and Zhang et al [30]).

To date, the most relevant solution has been proposed by Karmonik et al [31] who used 2D phase contrast MRI (1.5 T MRI) to observe wall displacement over the cardiac cycle on 7 patients (7 aneurysms) and 3 different locations (ACom, BA and ICA). This non-invasive technique was accurate enough to measure wall displacements as small as 0.04 mm, in the range of the expected wall displacement reported in our study. New generation MRI at 3T could offer a more accurate depiction of the wall motion in the next future.

As already stated, D_{max} gives local information about the wall displacement and in some cases, this parameter is not accurate enough to clearly demonstrate a difference between degraded/ruptured and non-degraded/unruptured aneurysms. The variation of the maximal mesh displacement measured by the software depends strongly of the displacement of the artery. The deformation of the artery induces an additional displacement of the mesh of the aneurismal sac. Then, the bulge of the artery is added to the displacement of the sac in relation to the artery to obtain the total maximal mesh displacement.

As shown in Table 4, the value of the ratio R_v is more important than R_d and allow us to better characterize aneurysm status. Furthermore, ΔV is a global indicator and is less sensitive to the uncertainties of the input parameters of the computations[14]. ΔV is thus thought to be a better parameter to evaluate the risk of rupture.

A limitation of this study was the simplification of the aneurismal environment in the FSI computations, by assuming that the aneurysm lies in a fluid of a given pressure. This environment would probably influence the geometrical variations of the aneurysm depending on the location: friction and contact of the wall with other structures (bone, meninges, arachnoid trabeculae, cerebrospiral fluid) will certainly impact on the wall motion [32, 33]. The assumptions made regarding the aneurysm wall is another limitation. In the present study, the aneurysm wall was considered as isotropic and homogenous but the anisotropy of this kind of biological material is well known [34]. Nevertheless, isotropy and homogeneity were assumed because they most probably do not change the trends observed when comparing soft and stiff materials in this range of physiological solicitation. To characterize the behavior of blood, more sophisticated models can be used in

order to account for non-Newtonian effects, especially in the aneurismal sac (Cebral *et al.*[35] and Sforza *et al.*[36]). However, these effects are expected to be prevalent only when dealing with local quantities like wall shear stress. This is not the case in the present study where the aneurismal volume, which is primarily influenced by the pressure forces generated by the blood flow, was analyzed.

Numerous parameters are not known precisely when computing the FSI problem for a specific patient: wall thickness, fluid boundary conditions, artery properties and intracranial pressure.

Despite these last limitations, the parametric study achieved in previous work[14] showed a positive consistency of our results regarding the numerous sources of uncertainty involved in such FSI computations. Therefore, the uncertainties of the input parameters did not change the main conclusion: whatever the values of the parameters (in a range of physiological variations), the soft/ruptured aneurysms deform more than the stiff/unruptured ones.

5 Conclusion

The difference in aneurismal pulsatility as highlighted in this work might be a relevant patient specific predictor of aneurysm rupture. These results are consistent with recent observational data in the literature to date. Development of new imaging technique would allow in the near future to accurately measure wall motion and therefore to characterise the intracranial aneurysm vulnerability for any given patient.

6 Acknowledgments

The authors thank Philips Healthcare, Inc. for the financial support and Ansys, Inc. for their technical support. The authors are also grateful to Simpleware, Inc. for providing the software Scan IP and for their technical support.

Table 1: Material coefficients of the aneurysm walls used in the present study

Aneurysm	C_{10} *(Mpa)*	C_{01}*(Mpa)*	C_{11}*(Mpa)*
Soft	0.024	0.026	0.42
Stiff	0.39	0	22.14

Table 2: Aneurysm geometry informations, with V the diastolic volume, D the dome size, N the neck size and D/N the ratio Dome/Neck.

aneurysm	**location**	**V (mm^3)**	**shape**	**D (mm)**	**N (mm)**	**D/N**
1	MCA R	61	Simple	4.8	4	1.2
2	MCA L	51	Complex	3.4	3.75	0.91
3	ACA	161	Simple	5.25	5.6	0.94
4	MCA R	188	Complex	5.5	6.5	0.85
5	ICA	392	Complex	9.2	5	1.84
6	VA	45	Simple	4	2.3	1.74
7	MCA L	212	Complex	7.8	6.6	1.18
8	ACA	232	Complex	8	4.5	1.78
9	ACA	79	Complex	6.85	2.9	2.36
10	OA	138	Simple	6.1	4.3	1.41
11	BA	68	Complex	4.4	3.9	1.13
12	BA	18	Simple	3	3	1

Table 3: Results of FSI computations for 12 different aneurysms for stiff and soft materials.

aneurysm	material	V (mm^3)	ΔV (mm^3)	Pulsatility = ΔV/V (%)	D_{max} (mm)
1	Soft	61	10	16	0.35
	Stiff		1	2	0.12
2	Soft	51	8	16	0.32
	Stiff		0.5	1	0.09
3	Soft	161	44	27	0.7
	Stiff		6	4	0.26
4	Soft	188	37	20	0.71
	Stiff		7	4	0.15
5	Soft	392	149	38	1
	Stiff		18	5	0.45
6	Soft	45	33	73	1.8
	Stiff		4	9	1.2
7	Soft	212	60	28	1.05
	Stiff		14	7	0.48
8	Soft	232	54	23	0.84
	Stiff		10	4	0.4
9	Soft	79	15	19	0.48
	Stiff		3	4	0.15
10	Soft	138	26	19	0.47
	Stiff		5	4	0.17
11	Soft	68	11	16	0.42
	Stiff		2.5	4	0.12
12	Soft	18	4	22	0.27
	Stiff		0.5	3	0.14

Table 4: Comparison between volumetric flow rate variation and volume variation of soft aneurismal sacs.

Aneurysm	**Systole flow rate ($m^3.s^{-1}$)**	**Flow rate variation ($m^3.s^{-1}$)**	**ΔV (mm^3)**
1	3.21 E-06	1.78 E-06	10
2	3.10 E-06	1.75 E-06	8
3	2.85 E-06	1.95 E-06	44
4	3.36 E-06	1.84 E-06	37
5	4.21 E-06	2.15 E-06	149
6	3.55 E-05	4.454E-05	33
7	3.12 E-06	1.77 E-06	60
8	1.28 E-06	1.27 E-06	54
9	1.62 E-06	7.94 E-07	15
10	2.92 E-07	1.36 E-07	26
11	5.07 E-06	3.34 E-06	11
12	5.07 E-06	3.34 E-06	4

Table 5: Results for R_v and R_d for the 12 cases

aneurysm	**Volume (mm^3)**	**$Rv = \Delta V^{soft} / \Delta V^{stiff}$**	**$Rd = D_{max}^{soft} / D_{max}^{stiff}$**
1	61	10	2.9
2	51	16	3.5
3	161	7.3	2.7
4	188	5.3	4.7
5	392	8.3	2.2
6	45	8.25	1.5
7	212	4.3	2.2
8	232	5.4	2.1
9	79	5	3.2
10	138	5.2	2.8
11	68	4.4	3.5
12	18	8	1.9

Figure 1: Nominal stress/engineering strain curves representing the average mechanical properties of the soft and the stiff classes.

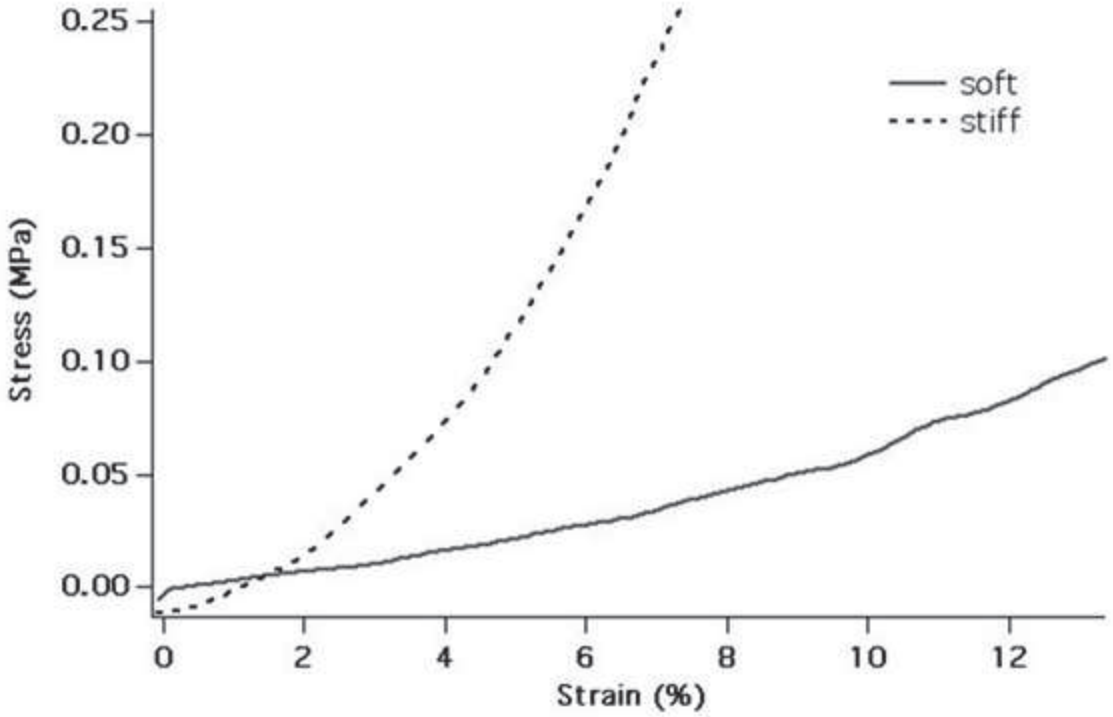

Figure 2: FSI maximal mesh displacement results for the systolic pressure for the aneurysms 10 (top), 8 (middle row) and 7 (bottom row) with the volumetric flow rate imposed at the inlet (On the left for the stiff material and on the right for the soft material).

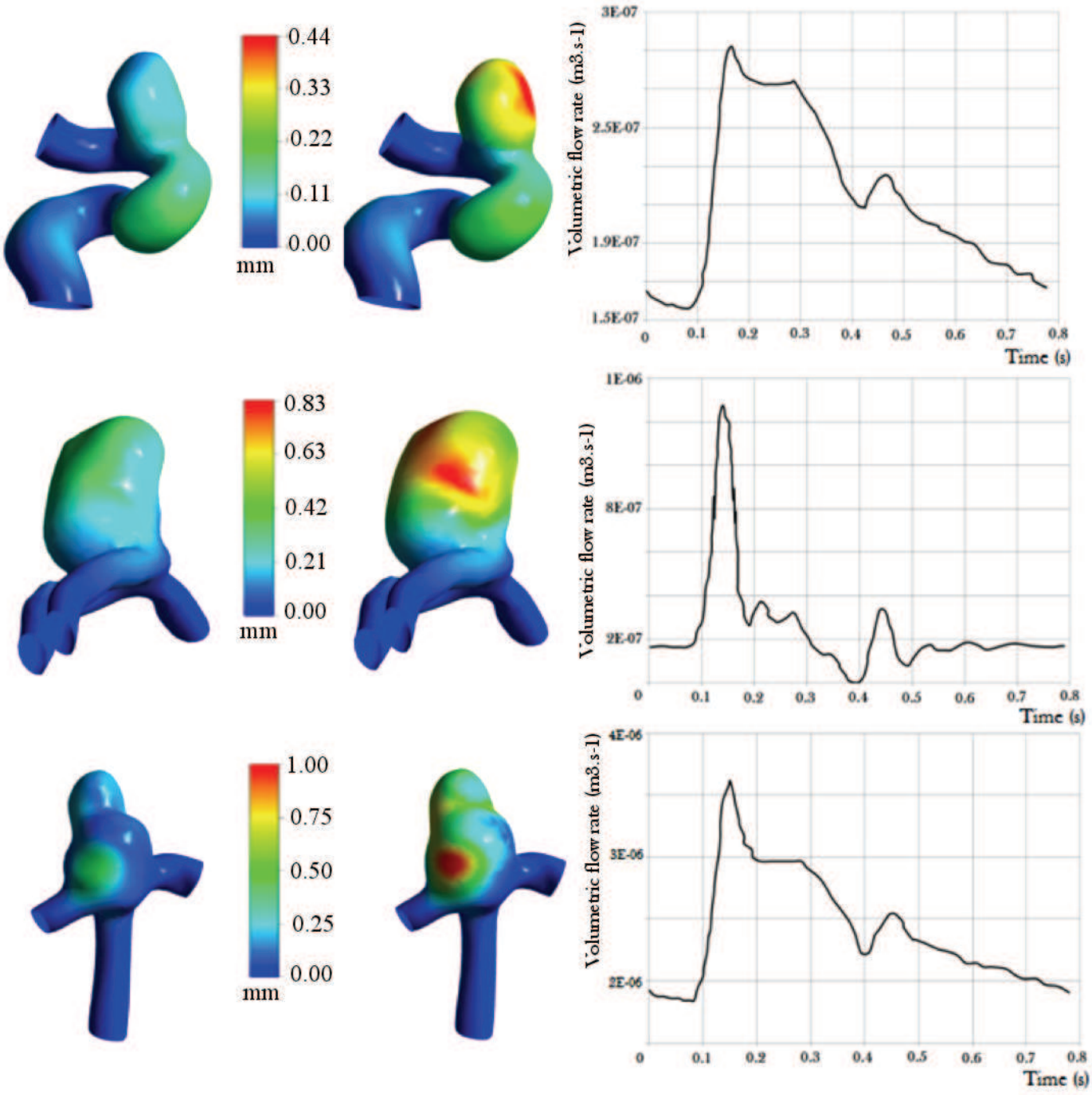

References

1. **Wardlaw J, White P. The detection and management of unruptured intracranial aneurysms. *Brain*. 2000;123:205 -221**
2. **Horikoshi T, Sugita M, Yagishita T, Nukui H. Size of cerebral aneurysms and related factors in patients with subarachnoid hemorrhage. *Surgical Neurology*. 2002;61:239 - 245**
3. **Nahed B, Diluna M, Morgan T, Ocal E, Hawkins A, Ozduman K, et al. Hypertension, age, and location predict rupture of small intracranial aneurysms. *Neurosurgery*. 2005;57:676 - 683**
4. **Matsubara S, Hadeishir H, Suzukil A, Yasui N, Nishimura B. Incidence and risk factors for the growth of unruptured cerebral aneurysms: Observation using serial computerized tomography angiography *Journal of Neurosurgery*. 2004;101: 908 - 914**
5. **Chung S, Vafai K. A coupling model for macromolecule transport in a stenosed arterial wall. 2012;45:371 - 381**
6. **Nicoud F, Moreno R, Tayllamin B, Chau M, Rousseau H. Computational hemodynamics in moving geometries without solving the fluid-structure interaction problem. *Conference on Modelling Fluid Flow 2009. The 14th International Conference on Fluid Flow Technologies. Budapest, Hungary, September 9-12, 2009*. 2009**
7. **Balocco S, Camara O, Vivas E, Sola T, Guimaraens L, Gratama van Andel H, et al. Feasibility of estimating regional mechanical properties of cerebral aneurysms in vivo. *Medical Physics*. 2010;37:1689-1706**
8. **Rissland P, Alemu Y, Einav S, Ricotta J, Bluestein D. Abdominal aortic aneurysm risk of rupture: Patient-specific fsi simulations using anisotropic model. *Journal of Biomechanical Engineering*. 2009;131:031001**
9. **Torii R, Oshima M, Kobayashi T, Takagi K, Tezduyar T. Fluid structure interaction modeling of a patient-specific cerebral aneurysm: Influence of structural modeling. *Computational Mechanics*. 2008;43:151 -159**

10. **Vito R, Hickey J. The mechanical-properties of soft-tissues. 2. The elastic response of arterial segments. *Journal of Biomechanics*. 1980;13:951 -957**

11. **Vande Geest J, Schmidt E, Sacks M, Vorp D. The effects of anisotropy on the stress analyses of patient-specific abdominal aortic aneurysms. *Annals of Biomedical Engineering*. 2008;36:921 - 932**

12. **Vande Geest J, Sacks M, Vorp D. The effects of aneurysm on the biaxial mechanical behavior of human abdominal aorta. *Journal of Biomechanics*. 2006;39:1324 - 1334**

13. **Costalat V, Sanchez M, Ambard D, al. Biomechanical wall properties of human intracranial aneurysms resected following surgical clipping. *Journal of Biomechanics*. 2011;44:2685 - 2691**

14. **Sanchez M, Ambard D, Costalat V, Mendez S, Jourdan F, Nicoud F. Biomechanical assessment of the individual risk of rupture of cerebral aneurysms: A proof of concept. *Annals of Biomedical Engineering*. 2013;41:28 - 40**

15. **Duprey A, Khanafer K, Schlicht M, Avril S, Berguer R. In vitro characterisation of physiological and maximum elastic modulus of ascending thoracic aortic aneurysms using uniaxial tensile testing. *European Journal of Vascular and Endovascular Surgery*. 2010;39:700-707**

16. **Ambard D, Cherblanc F. Mechanical behavior of annulus fibrosus: A microstructural model of fibers reorientation. *Annals of Biomedical Engineering*. 2009;37:2256 - 2265**

17. **Jourdan F, Samida A. An implicit numerical method for wear modeling applied to hip joint prothesis problem. *Computer Methods in Applied Mechanics and Engineering*. 2009;198:2209-2217**

18. **Malachanne E, Dureisseix D, Jourdan F. Numerical model of bone remodeling sensitive to loading frequency through a poroelastic behavior and internal fluid movements. *Journal of the Mechanical Behavior of Biomedical Materials*. 2011;4:849-857**

19. **Swider P, Pedrono A, Ambard D, Accadbled F, Sales de Gauzy J. Substructuring and poroelastic modelling of the intervertebral disc. *Journal of Biomechanics*. 2010;47:1287 -1291**

20. **Hoi Y, Meng H, Woodward S, Bendok B, Hanel R, Guterman L, et al. Effects of arterial geometry on aneurysm growth: Three-dimensional computational fluid dynamics study. *Journal of Neurosurgery*. 2004;101:676 - 681**

21. **Van de Vosse FS, N. Pulse wave propagation in the arterial tree. *Annu. Rev. Fluid Mech.* 2011;43:467-499**

22. **Steiner L, Andrews J. Monitoring the injured brain : Icp and cbf *British Journal of Anaesthesia*. 2006;97:26 - 38**

23. **Ai L, Vafai K. A coupling model for macromolecule transport in a stenosed arterial wall. *International Journal of Heat and Mass Transfer*. 2006;49:1568 - 1591**

24. **Watton P, Raberger N, Holzapfel G, Ventikos Y. Blood flow dynamics and fluid-structure interaction in patient specific bifurcating cerebral aneurysm *Journal of Biomechanical Engineering*. 2009;131: 1 - 14**

25. **Yang N, Vafai K. Modeling of low-density lipoprotein (ldl) transport in the artery- effects of hypertension. *International Journal of Heat and Mass Transfer*. 2006;49:850 - 867**

26. **Valencia A, Ledermann D, Rivera R, Bravo E, Galvez M. Blood flow dynamics and fluid-structure interaction in patient specific bifurcating cerebral aneurysm *International Journal for numerical methods in fluids*. 2009;58:1081 - 1100**

27. **Alnaes M, Isaksen J, Mardal K, Romner B, Morgan M, Ingebrigtsen T. Computation of hemodynamics in the circle of willis. *Stroke*. 2007;38:2500 - 2505**

28. **Hayakawa M, Maeda S, Sadato A, Tanaka T, Kaito T, Hattori N, et al. Detection of pulsation in ruptured and unruptured cerebral aneurysms by electrocardiographically gated 3-dimensional computed tomographic angiography with a 320- row area detector computed tomography and evaluation of its clinical usefulness. *Neurosurgery*. 2011;69:843 - 851**

29. **Ishida F, Ogawa H, Simizu T, Kojima T, Taki W. Visualizing the dynamics of cerebral aneurysms with four- dimensional computed tomographic angiography. *Neurosurgery*. 2005;57:460-471**

30. **Zhang C, Villa-Uriol M, Craene M, Pozo J, Frangi A. Morphodynamic analysis of cerebral aneurysm pulsation from time-resolved rotational angiography. *Medical Imaging*. 2009;28:1105 -1116**

31. **Karmonik C, Diaz O, Grossman R, Klucznik R. In vivo quantification of wall motion in cerebral aneurysm from 2d cine phase contrast magnetic resonance images. *Rofo*. 2010;182:140-151**

32. **San Millan Ruiz D, Yilmaz H, Dehdashti A, Alimenti A, de Tribolet N, R\ddotufenacht D. The perianeurysmal environment: Influence on saccular aneurysm shape and rupture. *American Journal of neuroradiology*. 2006;27:504-512**

33. **Seshaiyer P, Humphrey J. On the potentially protective role of contact constraints on saccular aneurysms. *Journal of Biomechanics*. 2001;34:607-612**

34. **MacDonald D, Finlay H, Canham P. Directional wall strength in saccular brain aneurysms from polarized light microscopy. *Annals of biomedical engineering*. 2000;28:533-542**

35. **Cebral J, Castro M, Putman C, Millan D, Frangi A. Efficient pipeline for image-based patient-specific analysis of cerebral aneurysm hemodynamics: Technique and sensitivity. *IEEE Transactions of Medical Imaging*. 2005;24:457 - 467**

36. **Sforza D, Putman C, Cebral J. Hemodynamics of cerebral aneurysms. *The Annual Review of Fluid Mechanics*. 2008;41:91 - 107**